Temperature-controlled growth of single-crystal Pt nanowire arrays for high performance catalyst electrodes in polymer electrolyte fuel cells

Yaxiang Lu, Shangfeng Du *, Robert Steinberger-Wilckens

School of Chemical Engineering, University of Birmingham, Edgbaston, Birmingham B15 2TT, UK

ABSTRACT

The anisotropic structure and unique surface properties of one-dimensional (1D) Pt-nanowire (PtNW) make it a promising new type of electrocatalyst for various catalyst applications, especially for fuel cells. However, due to the critical synthesis process, a finely tuning of the synthesis temperature for precisely controlling the morphology and distribution of PtNWs in catalyst electrodes still remains a grand challenge. In this work, we present the temperature-controlled growth of PtNWs with large-area $16\,cm^2$ carbon paper piece as a direct support. The relationship between the growth temperature and PtNW behavior is studied by physical characterization, and their catalytic activity is measured towards oxygen reduction reaction (ORR) by testing as the cathode in a hydrogen-air fuel cell. The results show that the growth temperature plays a vital role on the behavior of PtNWs thus influencing their properties. The catalyst electrode with PtNWs grown at $40\,°C$ shows the best power performance. A possible mechanism for the influence of temperature on PtNW growth is suggested. The comparison with the state-of-the-art commercial TKK catalyst also shows a better performance and durability. The understanding gained in our work from PtNW catalyst electrode could aid in the design of other novel nanostructures in practical applications.

1. Introduction

In the past decades, studies have been intensively conducted for the development of high performance electrocatalysts with novel nanostructures [1,2]. Previous results have established that the electrocatalytic activity and durability of electrocatalysts not only depends on the ratio of surface area to volume, but also arrangements of atoms, the surface structures and their morphologies [3]. For example, the high surface energy of extremely small nanoparticles often induces severe aggregation and Ostwald ripening, which are considered as two of the main contributors to the fast drop of power output and significant degradation of cycling life [4,5]. Compared with zero-dimensional (0D) nanoparticles, one-dimensional (1D) Pt nanostructures such as nanowires and nanotubes, benefiting from the inherent structural characteristics like anisotropy and preferential exposure of highly active crystal facets, exhibit enhanced catalytic activity and durability [6,7]. Lee et al. [8] synthesized single-crystal Pt nanowires on Pt and W gauzes, which

showed excellent catalytic activities towards oxygen reduction reaction (ORR) and methanol oxidation reaction (MOR). Liang et al. [9] prepared a free-standing Pt nanowire membrane and demonstrated that the 1D nanostructure displayed remarkably higher catalytic stability than Pt/C and Pt black.

In the synthesis of nanostructures, reaction temperature has been regarded as an important controlled factor. Controlling temperature is a good tool to tune the phase formation kinetics [10] and the driving force for mass transfer [11], thus changing the morphology and property of the product. Unfortunately, up to today, most studies related to Pt nanowires only focused on a fixed temperature, because it has been usually agreed that a relative low reaction temperature is necessary to slow down the reduction rate of Pt ions, favouring the growth of {1 1 1} planes and therefore leading to the formation of single-crystal Pt nanowires [5,12]. For instance, at room temperature, Sun et al. [12] synthesized single-crystal Pt nanowires on carbon black via the reduction of H_2PtCl_6 by HCOOH. At $110\,°C$, Xia and co-workers [8] grew Pt nanowires on metal gauzes by reducing H_2PtCl_6 with ethylene glycol in the presence of polyvinyl pyrrolidone (PVP). However, in the synthesis of nanostructures, the growth temperature also plays a key role on the behavior, e.g. distribution and aggregation of nanostructures. In

* Corresponding author. Tel.:+44 121 4145081.
 E-mail address: s.du@bham.ac.uk (S. Du).

practical applications, the behavior of Pt nanowires is as important as the Pt nanowires themselves. For example, when Pt nanowires are used as electrocatalysts in fuel cells, they should possess an optimal distribution in the catalyst layer to achieve a low charge and mass transfer resistance [13], a suitable length to enable self-support [14], and an ultra-thin size to obtain a high electrochemical surface area [15]. This highlights the importance of a finely tuned synthesis temperature for simultaneously controlling the behavior and structure of Pt nanowires for practical applications.

To further understand the influence mechanism of the growth temperature on the behavior and structure of Pt nanowires, in this work, Pt nanowires in situ grown on large-area carbon paper were investigated at different growth temperatures. Considering the real power performance in fuel cells, the role of the reaction temperature in the Pt nanowire growth process is proposed based on their morphology and distribution on support surface.

2. Experimental

2.1. Chemicals and materials

All chemicals and materials were used as received without any further purification. Hexachloroplatinic acid hexahydrate ($H_2PtCl_6 \cdot 6H_2O$, $\geq 37.50\%$ Pt basis) and formic acid (CH_2O_2, 98%) were purchased from Sigma-Aldrich UK. Isopropanol (C_3H_8O, >99.5%) was obtained from Fisher Scientific UK. DuPont Nafion® 212 membrane and Nafion® solution (D1021, 10 wt%) were purchased from Ion Power Inc. Sigracet 35 BC carbon paper was used as the fuel cell gas diffusion layer (GDL) and the support for Pt nanowire growth. The gas diffusion electrode (ELE1065-0983, 0.4 mg$_{Pt}$ cm^{-2}) was obtained from Johnson Matthey Fuel Cells Ltd and used as anode for fabricating fuel cells. Commercial 45.91 wt% Pt/C (TEC10E50E) catalyst was purchased from Tanaka Kikinzoku Kogyo K. K. (TKK) Japan. Ultrapure water (18.2 MΩ cm) from a Millipore water system was used throughout.

2.2. PtNW GDEs preparation and physical characterization

Pieces of 4 cm × 4 cm Sigracet 35BC carbon paper were used as the support for Pt nanowire growth. The detailed procedure is described in our previous studies [16,17]. Typically, to grow 0.4 mg cm^{-2} Pt nanowires on a piece of 16 cm^2 carbon paper, 17 mg $H_2PtCl_6 \cdot 6H_2O$ (6.4 mg Pt) and 0.53 mL formic acid were added to the 10.6 mL ultrapure water. The carbon paper was immersed in the mixed solution in a 6 cm glass Petri dish and stored at a respective temperature for Pt nanowire growth. After the colour of the solution changed from yellow to colourless and the growth of nanowires was completed, the samples were rinsed using ultrapure water and IPA, followed by drying at 40 °C overnight. The as-prepared carbon paper samples with in-situ grown Pt nanowires were directly used as gas diffusion electrodes (GDEs) at the cathode side. The morphology and distribution of Pt nanowires in GDEs were analysed with a field emission scanning electron microscope (FE-SEM, JEOL 7000F, operating at 20 kV) and a high-resolution transmission electron microscope (HR-TEM, Philips CM200). X-ray diffraction (XRD) patterns of the as-prepared GDEs were obtained with a Siemens D5005 powder X-ray diffractometer using Cu Kα (λ = 0.15418 nm) radiation operated at 40 kV and 30 mA. Thermogravimetry analysis (TGA) (NETZSCH, TG209F1 under a 40 ml min^{-1} air flow rate) was carried out to measure the actual loading of Pt nanowires in GDEs with a heating rate of 10 °C min^{-1} to 900 °C.

2.3. Membrane electrode assembly (MEA) fabrication

The commercial Johnson Matthey GDEs with a Pt nanoparticle loading at 0.4 mg$_{Pt}$ cm^{-2} were used as anodes and the as-prepared GDEs were used as cathodes. Before being fabricated into MEAs, the GDE surface was coated with a thin layer of Nafion ionomer. The two GDEs were then sandwiched at both sides of a 6 cm × 6 cm Nafion 212 membrane and the membrane electrode assembly (MEA) was hot pressed at 125 °C under 4.9 MPa pressure for 2 min. For comparison, a MEA with a cathode with the state-of-the-art commercial TKK Pt/C catalyst (0.4 mg$_{Pt}$ cm^{-2}) was fabricated simultaneously.

2.4. Fuel cell tests

The fabricated MEAs were tested in a PEM fuel cell stand (PaxiTech-BioLogic FCT-50S) with electrochemical impedance spectroscopy (EIS) capabilities. The gasket used in fuel cell testing is polytetrafluoroethylene (PTFE) sheet with a thickness of 254 μm at both cathode and anode sides. The MEA was activated by a break-in at 0.6 V for 7 h, and after that polarization curves were recorded at a scan rate of 1 mV s^{-1}. The gas flow rates for H_2 and air were at least 120 and 300 mL min^{-1} with a stoichiometry of 1.3/2.4, respectively. EIS measurements were performed in the frequency range from 10 kHz to 0.1 Hz with an amplitude of 10 mV. Cathode cyclic voltammograms (CVs) were recorded using an EZstat-Pro system integrated with the test stand. The cathode was fed with fully humidified pure nitrogen at 300 mL min^{-1}, and the anode was fed with fully humidified pure hydrogen at a flow rate of 120 mL min^{-1} serving as both reference and counter electrode, also designated as a dynamic hydrogen electrode (DHE). Then the cathode potential was cycled between 0.05 and 1.2 V versus DHE at 20 mV s^{-1} for 5 cycles, and the fifth cycle was recorded. Accelerated durability tests (ADT) were undertaken by continuous cyclic voltammetry cycling between 0.6 and 1.2 V for 2000 cycles at a scan rate of 50 mV s^{-1}. All the above mentioned tests were conducted at 70 °C with gases humidified at 75 °C before entering the cell and the backpressure was 2 bars at both sides.

Catalytic activity on oxygen was measured according to the method described in detail by Gasteiger et al. [18], considering the ohmic resistance correction and H_2 crossover correction. The catalyst testing was conducted in fuel cells at 80 °C with fully humidified H_2 and O_2. Stoichiometric flow rates of anode ($s = 2$) and cathode ($s = 9.5$) reactants were used at a minimum 120 and 300 mL min^{-1} to meet the requirement of the testing system. The total pressure was 1.5 bars at both sides for the whole testing process. Cell resistances were determined by in situ EIS measurement evaluated at 1 kHz and used for iR correction to the obtained cell voltage. The H_2 crossover correction was processed by including the H_2 crossover current densities measured at 0.6 V over a period of 30 min under the operating conditions (i.e., temperature and partial pressure) with fully humidified H_2 and N_2 purged at anode and cathode, respectively [19]. Catalyst activities were evaluated on the basis of ohmic resistance and H_2 crossover corrected current densities.

3. Results and discussion

Pt nanowires grown at various temperatures including 5, 15, 25, 35, 40 and 50 °C were investigated in this work. Too high temperature, e.g. 80 °C [20] will lead to a direct formation of Pt nanoparticles in solution by homogeneous nucleation, so the temperature range was chosen to be below 50 °C in this work. Fig. 1 shows SEM and TEM images of Pt nanowires grown at a low temperature of 5 °C. At such a low temperature, a big difference was observed to the Pt nanostructures and their distribution formed between the center and edge area in a 16 cm^2 GDE. Pt nanostructures are very sparse at the centre area (Fig. 1a and b) but showing an extremely high density at the edge area (Fig. 1d and e). At the centre area, most of the very sparse Pt nanowires assembled together to form small superstructure with size of ca. 100 nm. TEM analysis indicates the
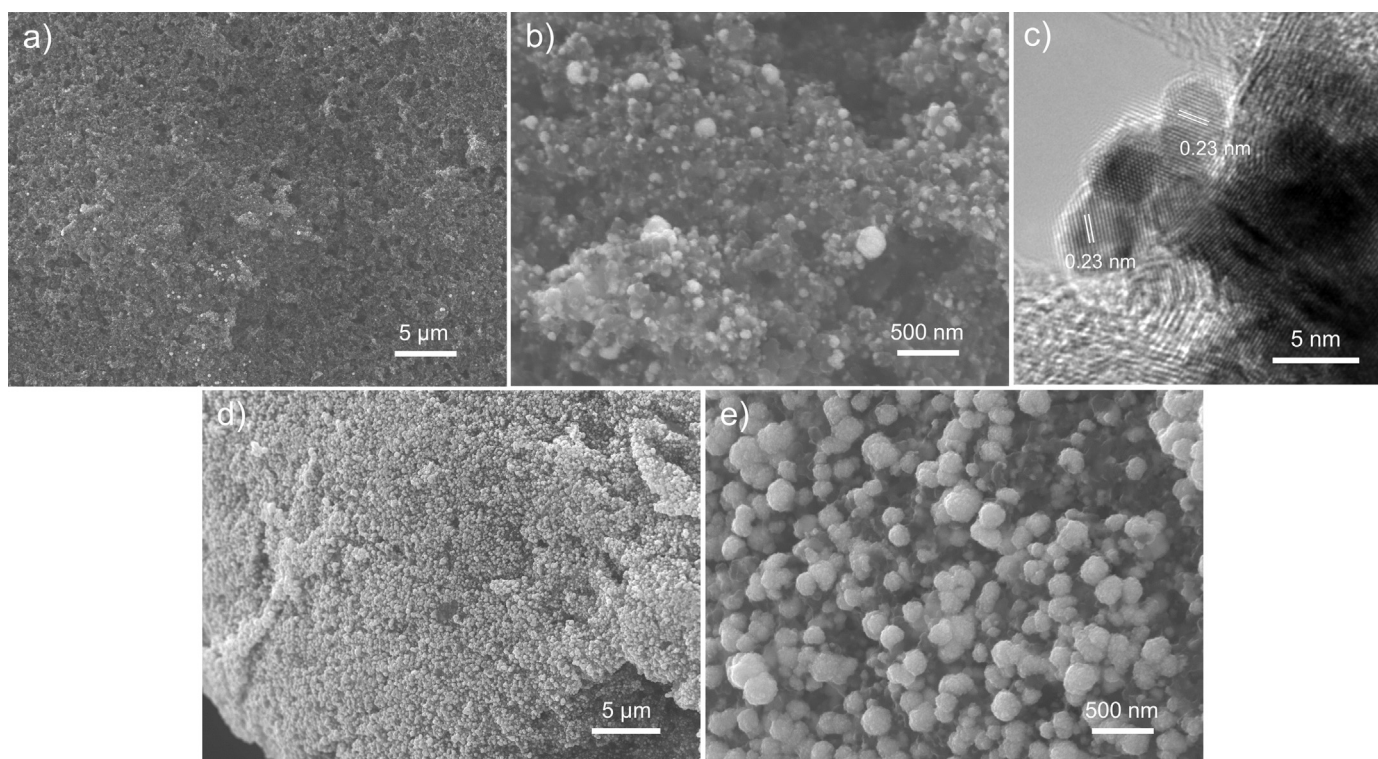
Fig. 1. (a and b, d and e) SEM and (c) TEM images of PtNW GDE grown at 5 °C. (a and b, d and e) show the centre and edge area of the GDE piece, respectively.

agglomeration of the very short Pt nanowires (Fig. 1c). The lattice space of 0.23 nm between the {1 1 1} planes is in agreement with that of the bulk Pt crystal. But at the edge area, the behavior of Pt nanowires is completely different, where they constructed together to form huge dense aggregates with size of about 0.5 μm or even large. This structure would significantly reduce the contribution of Pt to catalytic activity, resulting in a very low catalyst utilization.

With the increase of the reaction temperature, e.g. at 25 °C which is a common temperature used for growing Pt nanowires with this formic acid approach [12], more Pt nanowires were grown in the centre of the GDE compared with that at 5 °C, as shown in Fig. 2a and b. This improvement reduced the large aggregates at edge area, bringing in a higher catalyst utilization. When the temperature continued to increase, e.g. at 50 °C, it is enough to overcome the homogenous nucleation energy barrier in solution, thus nanoparticles rather than nanowires were produced. Fig. 2c shows that a lot of small nanoparticles pile up on the GDL surface, which had a particle size of a few nanometers. This thick layer of nanoparticles would partially block the oxygen diffusion in the fuel cell operation thus resulting in a large mass transfer resistance.

An optimal temperature of 40 °C was achieved in this work. As can be seen from SEM images shown in Fig. 3a–c, uniform Pt nanowire arrays were attained through the entire surface of 16 cm^2 carbon paper. HR-TEM image (Fig. 3d) further shows that Pt nanowires have a length of 10–20 nm which was longer than those at lower temperature. A magnified image shown in Fig. 3e displays the crystallographic alignment of Pt nanowires and demonstrates the single crystallinity. In this case, the advantages of the Pt nanowires can be maximized, and an excellent catalytic performance is expected.

It can be seen that the growth temperature plays a key role not only on PtNW nanostructure, but also on their behavior including distribution and aggregation. As we know, in the synthesis of nanostructures by wet chemical process, the nucleation can start in the reaction solution by homogeneous nucleation [21], or on

the rough sites at the support surface by heterogeneous nucleation [22]. The heterogeneous nucleation usually needs a lower energy than homogenous nucleation [23], but subjected to the barrier existed and energy provided for nucleation in the system [24]. In GDL carbon paper, the top layer is mainly constructed by carbon nanospheres. The surfaces of these carbon nanospheres are inert where a surface modification is usually needed if using specially as catalyst support [25,26]. Furthermore, to prevent the water flooding in fuel cell operation, GDL carbon paper is usually treated with polytetrafluoroethylene (PTFE) for a super hydrophobicity. In this case, at a low temperature, the high surface tension of the aqueous reaction solution can't wet the GDL support surface very well, in particular at the center area for such a large piece [27], thus the active sites provided on surface for nucleation are very limited. Furthermore, the very low temperature also significantly slows down the crystal growth rate [28]. Hence, the main structures obtained were large dense aggregates from the short Pt nanowires at the edge area and very few Pt nanowires grew in the center area, as seen in Fig. 1. With the increase of reaction temperature, the surface tension of water reduced and led to a decrease of water contact angle, thus the wettability on the support surface was improved [27]. Therefore, in the centre area, the population of the nucleation cites multiplied and more Pt nanowires were obtained, as observed for PtNW GDEs grown at the medium temperature. At an optimal range, e.g. 40 °C here, uniform PtNWs were grown on the carbon paper surface, as seen in Fig. 3. However, when the temperature reached a very high point, e.g. 50 °C, the energy provided in the system would be large enough to overcome the barrier for homogeneous nucleation, and then nuclei would be formed in solution [29,30]. It is also known that the crystal growing is very fast at a high temperature [28]. In this case, nanoparticles will be obtained rather than nanowires due to the fast crystal growth rate and the large amount of nuclei formed. This approach has been widely used to synthesize small nanoparticles [31]. Therefore, in our work here, even more nucleation sites obtained on carbon paper surface, a
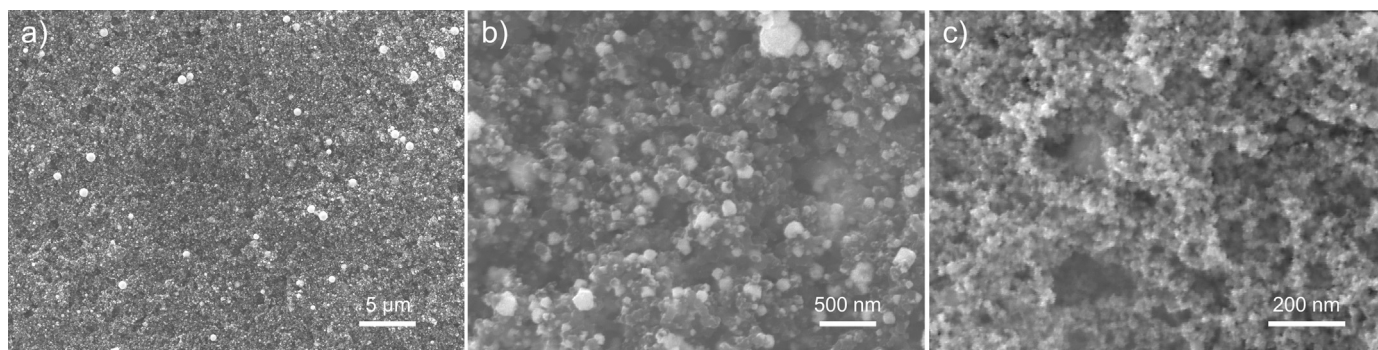
Fig. 2. SEM images showing the center area of a 16 cm^2 PtNW GDE grown at (a and b) 25 °C, at two different magnifications, and (c) 50 °C.

uniform growth of Pt nanowires still could not be achieved. Some of these Pt nanoparticles formed in solution would then partially deposit and pile up on the support surface, as shown in Fig. 2c. In experiment, it was also noticed that the reactant solution became dark at 50 °C, indicating the direct formation of Pt nanoparticles in the solution. The thick Pt nanoparticle layer in GDE will block the oxygen transfer in operation, in addition to the loss of Pt nanoparticles in solution, thus a poor catalyst electrode performance is as expected. Hence, to achieve uniform Pt nanowires with good distribution, surface structure and morphology on support surface, an optimal temperature is necessary to effectively control the Pt nucleation and crystal growth in the reaction system. In our work here, this was achieved at 40 °C. A schematic diagram is shown in Fig. 4 to explain the growth mechanism of Pt nanowires on the carbon paper surface at low, moderate and high temperatures.

XRD analysis was also conducted to 35BC GDL and PtNW GDEs grown at 5, 25, 40 and 50 °C to confirm the crystallinity of Pt nanowires (Fig. 5a). The diffraction peaks observed at 39.5°, 46.8° and 67.6° corresponds to the (1 1 1), (2 0 0) and (2 2 0) planes of the face-centred cubic (fcc) structure of Pt, indicating that PtNWs have a similar crystalline structure to the bulk Pt. TGA was implemented for PtNW GDE grown at 40 °C to measure the actual Pt loading (Fig. 5b). The residue shows a Pt loading of 6.38 mg on the 16 cm^2 GDL, which is very close to the expected 6.4 mg Pt amount, demonstrating that almost all of the PtNWs were grown on the GDL support.

In order to understand the effect of PtNW behavior on the practical catalytic performance, PtNW GDEs fabricated at various temperatures from 5 to 50 °C were used directly as cathodes and tested in hydrogen-air polymer electrolyte fuel cells (PEFCs) with an active area of 16 cm^2. Fig. 6a shows the polarization curves of the MEAs with the as-prepared PtNW GDEs. The one grown at 5 °C showed a very poor performance. With the increase of temperature, a better power performance was obtained, reaching the
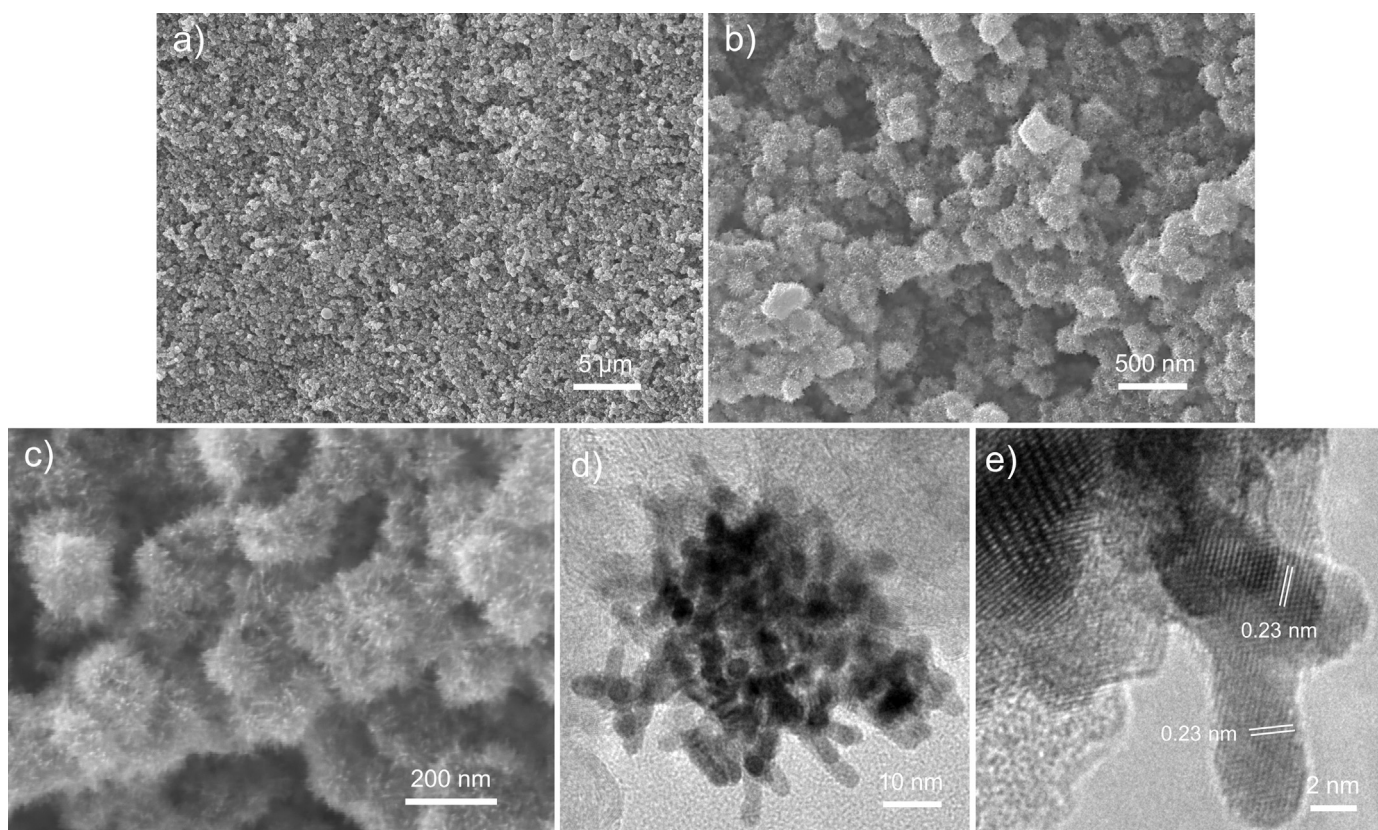

Fig. 3. (a–c) SEM images showing the centre area of PtNW GDE grown at 40 °C. (d and e) Shows TEM images of PtNWs.
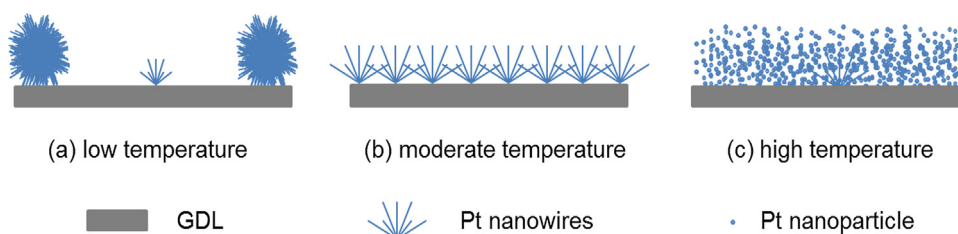
Fig. 4. Schematic diagram for Pt nanostructures grown on carbon paper surface at (a) low, (b) moderate and (c) high temperatures.

maximum value at 40 °C. The power density at 0.6 V increased from 0.51 W cm^{-2} at 5 °C to 0.82 W cm^{-2} at 40 °C. A higher temperature led to a rapid decrease on the electrode performance, dropping to only 0.54 W cm^{-2} (at 0.6 V) at 50 °C. It is worthy of noting that there was no big change on power performance for PtNW GDEs grown in the medium temperature range from 15 to 35 °C. A comparison of the PtNW GDEs and a GDE with the state-of-the-art commercial TKK Pt/C catalyst (the same loading of 0.4 mg cm^{-2}) is also included in Fig. 6a. The commercial catalyst showed a lower power density at 0.6 V, which is 0.74 W cm^{-2}.

Cathode CVs were recorded for PtNW GDEs grown at 5, 25, 40 and 50 °C as well as that of the TKK Pt/C catalyst in the single cell to measure the electrochemical surface area (ECSA) of Pt. From CVs in Fig. 6b, based on the actual Pt loading from TGA, the calculated ECSAs for PtNW GDEs grown at 5, 25, 40, 50 °C and that of Pt/C catalyst are 15.04, 12.90, 34.37, 4.91 and 56.87 m^2 g$_{Pt}^{-1}$, respectively. TKK Pt/C catalyst has a very large ECSA, owing to the high surface area from its nanoparticle morphology. Despite of the heavy

aggregation of PtNWs in PtNW GDE grown at 5 °C, a similar CV was obtained to that of at 25 °C. Possible reason is that at low temperature, the length of PtNWs is very short (Fig. 1c) and a relative larger surface area was gained compared with a longer PtNWs. When temperature arrived to the optimal value at 40 °C, uniform PtNWs with very little aggregation covered the whole surface and a better ECSA was achieved as expected. At 50 °C, most Pt nanoparticles grew directly in the solution rather than on the GDL surface, and all of those deposited on GDL surface also piled together, finally resulting in a very low ECSA.

To further understand the PtNW behavior, EIS measurements were conducted for PtNW GDEs grown at 5, 25, 40 and 50 °C and the results are shown in Fig. 6c–e. The measurements were performed at three current densities at 0.05, 0.5 and 1.0 A cm^{-2}, corresponding to low, mid and high current density range, respectively. At a low current density, the main impedance was contributed by the charge transfer resistance shown by the diameter of the impedance semi-circle, indicating the catalytic kinetic performance [32,33]. It can be seen that the PtNW GDE of 40 °C showed the smallest charge transfer resistance, and the one of 5 °C exhibited a very large value. At a medium or large current density, the contribution from mass transfer resistance would dominate the impedance. During this range, the PtNW GDE of 40 °C still displayed the smallest first and second impedance semi-circles, indicating the smallest charge and mass transfer resistances, respectively. These are in agreement with the power performance obtained in Fig. 6a, benefiting from the regular distribution of PtNW arrays in the catalyst electrode. The one of 5 °C still exhibited the largest charge transfer resistance, indicating the poor catalytic performance caused by the huge PtNW aggregates; while the one of 50 °C presented the largest mass transfer resistance at the high current density, resulting from the thick catalyst layer of the piled up Pt nanoparticles in GDEs.

It could be seen that a temperature of 40 °C enabled the uniform growth of PtNWs to achieve the highest catalytic activity. To further confirm the excellent stability of the single-crystal PtNWs as reported in the literature [9,34] and their good contact with carbon paper support, accelerated durability test (ADT) was conducted to check the durability of the as-prepared PtNW GDE of 40 °C and commercial TKK Pt/C catalyst. The ADT was performed by 2000 potential sweeping cycles in real fuel cell conditions with cathode filling of humidified nitrogen gas. Fig. 6f shows the CVs before and after the durability test. After the ADT, the remained ECSA of PtNW GDE of 40 °C and Pt/C is 17.76 and 18.81 m^2 g$_{Pt}^{-1}$, corresponding to 48% and 67% loss in their ECSA value, respectively, which indicates the better durability of the PtNW GDE as compared with the nanoparticle one.

For a better understanding of the better intrinsic catalytic performance of PtNWs over Pt/C, the catalytic activity of TKK Pt/C and PtNWs grown at 40 °C was also tested in MEA using H$_2$/O$_2$ to minimize the ohmic and mass-transfer polarizations in GDEs. The kinetic catalytic activity was evaluated at 0.9 V from the H$_2$/O$_2$ performances after ohmic and H$_2$ crossover corrections [18,19]. The
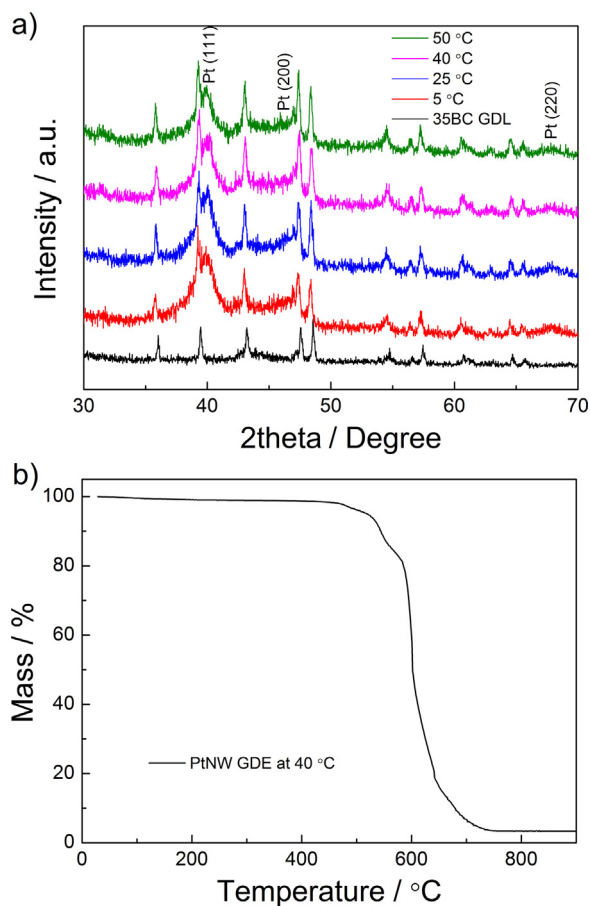

Fig. 5. (a) XRD patterns of 35BC GDL and PtNW GDEs grown at 5, 25, 40 and 50 °C; (b) TGA for PtNW GDE grown at 40 °C.
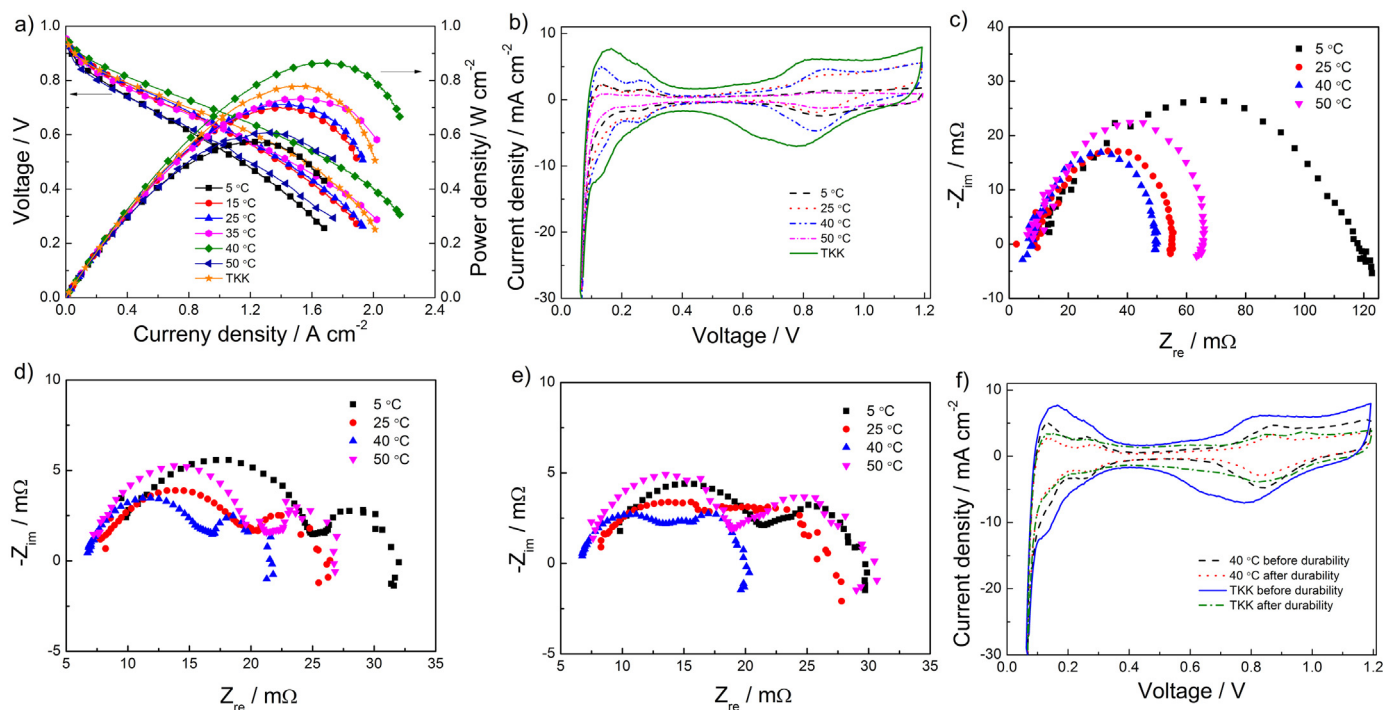
Fig. 6. (a) Polarization curves and (b) cathode cyclic voltammograms (CVs) of PtNW GDEs grown at different temperatures and the one with TKK Pt/C catalyst; (c–e) electrochemical impedance spectra (EIS) measured at (c) 0.05, (d) 0.5 and (e) 1.0 A cm^{-2} for PtNW GDEs grown at different temperatures; (f) cathode CVs before and after the accelerated durability test (ADT) for PtNW GDE grown at 40 °C and the electrode with TKK Pt/C catalyst.

Table 1
Catalytic performance characteristics of the two MEAs with TKK Pt/C and PtNW 40 °C described and shown in Fig. 7.

Catalysts	ECSA (m^2/g$_{Pt}$)	i (0.9 V) (mA/cm^2)	i_m (0.9 V) (A/mg$_{Pt}$)	i_s (0.9 V) (μA/cm$^2_{Pt}$)
TKK Pt/C	56.87	47.29	0.118	207.89
PtNW 40 °C	34.37	89.85	0.225	653.55

original uncorrected and corrected H$_2$/O$_2$ performance is shown in Fig. 7 and the results are summarized in Table 1. It can be seen that the mass activity of PtNW 40 °C, 0.225 A/mg$_{Pt}$ is nearly twice that of TKK Pt/C which is 0.118 A/mg$_{Pt}$, and a more than 3
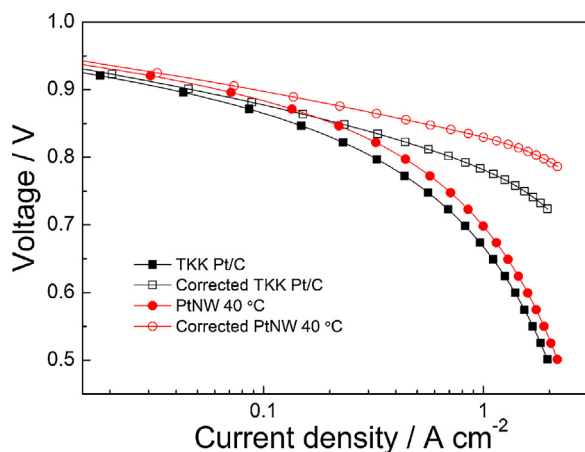

Fig. 7. Original uncorrected (solid square and circular symbols) and corrected (empty square and circular symbols) H$_2$/O$_2$ performance of the MEAs with the TKK Pt/C and PtNW GDEs. Measurements were taken at 80 °C with fully humidified reactants at 1.5 bar (H$_2$/O$_2$ stoichiometric flows of s = 2/9.5). The resistance-corrected cell voltage was determined via in situ EIS (evaluated at 1 kHz) vs. current density. Current densities were H$_2$ crossover corrected to yield the shown effective current density.

times higher specific activity is achieved which agrees very well with the data reported in the literature [18]. The kinetic activities obtained here are in line with the measured power performance above, further indicating the better catalytic activity of our PtNW catalysts.

4. Conclusions

In this study, we demonstrated the effect of the reaction temperature on the growth behavior of Pt nanowires with large-area 16 cm^2 carbon paper GDL as direct support. The experiment results indicated that the growth temperature plays a key role in this process. At the low temperature, the main structures obtained were huge PtNW aggregates, resulting in a low catalyst utilization and poor catalytic performance. An increased temperature brought in an improved distribution of PtNWs on the support surface. However, too high the reaction temperature resulted in the formation of nanoparticles in solution. At an optimal temperature of 40 °C, uniformly distributed PtNW arrays were achieved on the GDL surface, which showed the best catalytic performance in hydrogen/air fuel cell test. Benefiting from the enhanced intrinsic catalytic activity of PtNWs and the improved mass transfer polarization of the PtNW GDE, a higher power density of 0.82 W cm^{-2} was obtained at 0.6 V compared with 0.74 W cm^{-2} of the commercial TKK Pt/C catalyst. The in situ H$_2$/O$_2$ testing also demonstrated a double mass activity and a three times higher specific activity of PtNW over TKK Pt/C, which were 0.225 A/mg$_{Pt}$ and 653.55 μA/cm$^2_{Pt}$. The as-prepared PtNW GDE at 40 °C also exhibited a better durability than the one with Pt/C nanoparticles, demonstrating a 48% and 67% ECSA loss after the durability test, respectively. Because other nanostructures face the same challenge as here in the synthesis, in particular on various support surfaces, our improved understanding here from PtNW GDEs could provide useful reference for research on novel nanostructures in fuel cells and other catalytical applications.

Acknowledgements

References

[1] S.K. Kamarudin, N. Hashim, Renew. Sust. Energy Rev. 16 (2012) 2494–2515.
[2] S. Zhang, Y.Y. Shao, G.P. Yin, Y.H. Lin, J. Mater. Chem. A 1 (2013) 4631–4641.
[3] Y.H. Bing, H.S. Liu, L. Zhang, D. Ghosh, J.J. Zhang, Chem. Soc. Rev. 39 (2010) 2184–2202.
[4] P.J. Ferreira, G.J. la O', Y. Shao-Horn, D. Morgan, R. Makharia, S. Kocha, H.A. Gasteiger, J. Electrochem. Soc. 152 (2005) A2256–A2271.
[5] S.H. Sun, G.X. Zhang, D.S. Geng, Y.G. Chen, R.Y. Li, M. Cai, X.L. Sun, Angew. Chem. Int. Ed. 50 (2011) 422–426.
[6] S. Du, Int. J. Low-Carbon Technol. 7 (2012) 44–54.
[7] B. Lim, M.J. Jiang, P.H.C. Camargo, E.C. Cho, J. Tao, X.M. Lu, Y.M. Zhu, Y.N. Xia, Science 324 (2009) 1302–1305.
[8] E.P. Lee, Z.M. Peng, D.M. Cate, H. Yang, C.T. Campbell, Y.N. Xia, J. Am. Chem. Soc. 129 (2007) 10634–10635.
[9] H.W. Liang, X.A. Cao, F. Zhou, C.H. Cui, W.J. Zhang, S.H. Yu, Adv. Mater. 23 (2011) 1467–1471.
[10] A. Mallik, PhD Thesis, National Institute of Technology, India, 2010.
[11] J.H. ter Horst, D. Bedeaux, S. Kjelstrup, J. Chem. Phys. 134 (2011) 1–11.
[12] S.H. Sun, F. Jaouen, J.P. Dodelet, Adv. Mater. 20 (2008) 3900–3904.
[13] S.F. Du, B.G. Pollee, Int. J. Hydrogen Energy 37 (2012) 17892–17898.
[14] J.Y. Chen, B. Lim, E.P. Lee, Y.N. Xia, Nano Today 4 (2009) 81–95.
[15] R. Wang, D.C. Higgins, M.A. Hoque, D. Lee, F. Hassan, Z. Chen, Sci. Rep. 3 (2013) 1–7.
[16] S.F. Du, J. Power Sources 195 (2010) 289–292.
[17] S.F. Du, B. Millington, B.G. Pollet, Int. J. Hydrogen Energy 36 (2011) 4386–4393.
[18] H.A. Gasteiger, S.S. Kocha, B. Sompalli, F.T. Wagner, Appl. Catal. B-Environ. 56 (2005) 9–35.
[19] S.S. Kocha, in: W. Vielstich, A. Lamm, H. Gasteiger (Eds.), Handbook of Fuel Cells-Fundamentals, Technology and Applications, vol. 3, Wiley, Chichester, UK, 2003, p. 538 (chapter 43).
[20] A.L.N. Pinheiro, A. Oliveira-Neto, E.C. de Souza, J. Perez, V.A. Paganin, E.A. Ticianelli, E.R. Gonzalez, J. New Mater. Electron. Syst. 6 (2003) 1–8.
[21] D. Kashchiev, G.M. van Rosmalen, Cryst. Res. Technol. 38 (2003) 555–574.
[22] D.J. Srolovitz, G.S. Grest, M.P. Anderson, A.D. Rollett, Acta Metall. 36 (1988) 2115–2128.
[23] S. Puri, V.K. Wadhawan, Kinetics of Phase Transitions, first ed., CRC Press, Boca Raton, 2009.
[24] X.Y. Liu, J. Chem. Phys. 112 (2000) 9949–9955.
[25] P. Serp, M. Corrias, P. Kalck, Appl. Catal. A-Gen. 253 (2003) 337–358.
[26] P. Trogadas, T.F. Fuller, P. Strasser, Carbon 75 (2014) 5–42.
[27] K.Q. Li, X.R. Zeng, H.Q. Li, X.J. Lai, C.X. Ye, H. Xie, Appl. Surf. Sci. 279 (2013) 458–463.
[28] O. Song, Z.J. Zhang, J. Am. Chem. Soc. 126 (2004) 6164–6168.
[29] D.W. Oxtoby, J. Phys.: Condens. Matter 4 (1992) 7627–7650.
[30] M.V. Massa, K. Dalnoki-Veress, Phys. Rev. Lett. 92 (2004) 91–94.
[31] J.Y. Chen, T. Herricks, M. Geissler, Y.N. Xia, J. Am. Chem. Soc. 126 (2004) 10854–10855.
[32] L.H. Qiu, Y.J. Peng, B.Q. Liu, B.C. Lin, Y. Peng, M.J. Malik, F. Yan, Appl. Catal. A-Gen. 413 (2012) 230–237.
[33] X.Y. Yao, K.H. Su, S. Sui, L.W. Mao, A. He, J.L. Zhang, S.F. Du, Int. J. Hydrogen Energy 38 (2013) 12374–12378.
[34] Z.W. Chen, M. Waje, W.Z. Li, Y.S. Yan, Angew. Chem. Int. Ed. 46 (2007) 4060–4063.